

ARTICLES

 $^1\text{H}(d, 2p)n$ reaction at 2 GeV deuteron energy

J. Erő, Z. Fodor, P. Koncz, and Z. Seres

KFKI Research Institute for Particle and Nuclear Physics, 1525 Budapest, Hungary

C. F. Perdrisat and V. Punjabi*

College of William and Mary, Williamsburg, Virginia 23185

A. Boudard, B. Bonin, M. Garçon, R. Lombard, B. Mayer, Y. Terrien, and E. Tomasi

Département de Physique Nucléaire, Moyennes Energies, Centre Etudes Nucleaires, Saclay, 91191 Gif-sur-Yvette, France

M. Boivin and J. Yonnet

Laboratoire National Saturne, Saclay, 91191 Gif-sur-Yvette, France

H. C. Bhang and M. Youn

Seoul National University, Seoul 151-742, Korea

S. L. Belostotsky, O. G. Grebenuk, V. N. Nikulin, and L. G. Kudin

St. Petersburg Nuclear Physics Institute, Gatchina, 188350 Russia

(Received 16 March 1994)

The $^1\text{H}(d, 2p)n$ deuteron breakup reaction was measured at 2 GeV deuteron energy in a kinematically complete experiment. Fivefold differential cross sections are given in a wide range of kinematical variables and analyzed in terms of impulse approximation and NN rescattering. The deuteron momentum density was determined and deviations were found depending on the value of the four-momentum transfer $|t|$ in the scattering process. At low $|t|$ the momentum densities are in good agreement with the impulse approximation whereas large discrepancies were found above $q \approx 200$ MeV/c when the four-momentum transfer was large. Various possible origins of the anomalous behavior at high q values are discussed.

PACS number(s): 25.45.-z, 25.10.+s

I. INTRODUCTION

The wave function of the deuteron has been the subject of many investigations, in order to obtain information on the bound two-nucleon system at low as well as at high values of the internal momentum. Three kinds of experiments were usually performed in these studies: kinematically complete measurements of the deuteron breakup reaction induced by electrons and that induced by protons and the $A(d, p)X$ type inclusive experiments detecting the breakup products in the interaction of deuterons with different target nuclei. The bombarding energies varied from several hundred MeV up to 7.4 GeV.

In the $^2\text{H}(e, ep)n$ and $^2\text{H}(p, 2p)n$ or equivalent reactions the leading process is the quasifree scattering of

the incoming particle on one of the deuteron's nucleons, leaving the momentum of the other nucleon (spectator) unchanged. This first order process will be referred to in the following as impulse approximation (IA). In this simplified description the momentum of the spectator nucleon in the rest frame of the deuteron is the same before and after the reaction and it can be identified as the internal momentum q in the deuteron. Although IA turned out to be a rather good approximation, secondary effects, e.g., rescattering or final state interactions, may give a significant background to the cross section. In the above-mentioned inclusive experiments the reaction mechanism is similar: the target nuclei are bombarded by high energy deuterons but after interaction only the spectator nucleon is detected, mostly at 0° to the beam direction. Its momentum distribution in the deuteron rest frame gives directly the deuteron single-nucleon momentum density $|\Phi(q)|^2$ in impulse approximation.

In the (e, ep) experiments the measured single-nucleon momentum density after the necessary corrections was found to be in good agreement with the theoretical one

*Present address: Department of Physics and Chemistry, Norfolk State University, 2401 Corprew Avenue, Norfolk, VA 23504.

calculated on the basis of reliable two-nucleon potentials. No significant deviations were observed even at internal momenta as high as 0.6 GeV/ c (Refs. [1–3]). On the other hand, in proton induced breakup reactions the agreement with theory was restricted to small internal momenta, and large deviations from the impulse approximation were observed especially at internal momenta above approximately 0.2 GeV/ c . This behavior of the breakup reactions seems to be quite general, it was found in kinematically complete experiments at different primary energies ranging from ~ 0.4 up to 1 GeV and under different kinematical conditions [4–6]. Till now only one exception was reported in an experiment performed at 1 GeV proton energy [7] when satisfactory agreement with IA was found up to 0.28 GeV/ c internal momenta. To understand the origin of this deviation the effects of multiple scattering, final state interactions, and possible Δ production were calculated but these corrections to IA did not provide a satisfactory explanation for the increased cross section at high q values.

Inclusive breakup experiments have been done in a wider energy range [8–11], from a kinetic energy of 1.25 GeV up to 7.4 GeV and in these cases the behavior of $|\Phi(q)|^2$ was found to be similar to the exclusive ($p, 2p$) measurements. Irrespective of the energy and the kind of target a relatively broad shoulder was observed at internal momenta $q \approx 0.3 - 0.35$ GeV/ c . In an experiment published in Ref. [11] with a polarized deuteron beam the tensor analyzing power T_{20} was also determined at 0° for the spectator protons. It was found that the value of T_{20} was in agreement with IA predictions up to $q \approx 0.2$ GeV/ c but markedly deviated from it at higher momenta.

The discrepancy in the deuteron internal momentum distribution observed in almost all experiments performed with nucleonic probes proved to be typical of this type of interaction. Although various approaches have been applied in an attempt to understand the origin of this anomaly, no satisfactory explanation for the universal presence of the shoulder in $|\Phi(q)|^2$ or for the behavior of T_{20} near $q = 0.3$ GeV/ c internal momenta have been found up till now.

Recently we investigated the $^1\text{H}(d, 2p)n$ breakup reaction in a kinematically complete, exclusive experiment at Saclay using 2 GeV vector and tensor polarized deuterons. The aim of the experiment was to study the structure of the deuteron wave function at large internal momenta by investigating polarization phenomena under definite kinematical conditions. It was found that the measured asymmetries and polarizations at low q values were in accordance with the predictions of the IA; at higher internal momenta, however, significant deviations were observed [12]. Although the measurement was primarily planned as a means of investigating polarization effects, information was also obtained on the variation of the cross section itself in an extended range of the kinematical variables. In the present article we deal with the unpolarized cross section results.

In Sec. II, the experimental setup and the data analysis will be described; experimental results are given in Sec. III. The discussion, comparison of the experimental

cross sections to theoretical predictions, and some conclusions are presented in Sec. IV.

II. EXPERIMENT AND DATA HANDLING

In this work the deuteron breakup reaction

$$d + p \rightarrow p + p + n \quad (1)$$

has been investigated in a kinematically complete (exclusive) experiment. To specify the particles involved in the reaction we will use the symbols and subscripts as follows:

$$(1) + (2) \rightarrow (3) + (4) + (5). \quad (2)$$

The experiment was performed at the Laboratoire National Saturne at Saclay. Vector and tensor polarized deuterons (particle 1) accelerated to $T_1 = 2$ GeV kinetic energy by the SATURNE synchrotron were directed to a liquid hydrogen target. The two scattered protons (particles 3 and 4) were detected by the SPES IV magnetic spectrometer and by a recoil spectrometer of large angular acceptance (RS), respectively.

The deuterons were accelerated in bursts of about 0.4 s duration and with about 3 s repetition time. Beam intensities 3.0×10^9 d/burst were typical. The target was a liquid-H₂ cell of 0.280 g/cm² thickness, with 0.032 g/cm² thick Mylar and 0.013 g/cm² thick Ti windows. Since the entire experiment was planned to investigate polarization phenomena, the successive beam bursts contained deuterons in periodically changing polarization states. Only the unpolarized cross sections summing up the events from bursts with different polarization states are dealt with here.

The forward going protons (particle 3) were detected by the SPES IV spectrometer at $\Theta_{30} = 18.3^\circ$ to the primary beam direction. The resolution of the spectrometer was typically 10^{-3} with a total momentum acceptance of 7%. Besides the momentum the spectrometer also determined the horizontal and vertical angles at the entrance providing an opportunity to subdivide the angular acceptances in the off-line evaluation process. Time-of-flight information served to select protons from the reaction products. More details on the spectrometer can be found in Grorud *et al.* [13].

The recoil protons (particle 4) were detected by the RS, with its symmetry axis at $\Theta_4 = -57.0^\circ$ in the horizontal plane. This spectrometer consisted of two sets of multiwire proportional chambers (MWPC1 and MWPC2 — each composed of a vertical and a horizontal chamber), an array of 7 scintillation plates for ΔE measurements, and a 7×4 matrix of scintillation blocks to obtain energy information. The distances between the target and MWPC1 and MWPC2 were 1.2 m and 2.7 m, respectively, which together with the 4 mm spacings between the sense wires, defined the angular resolution as $\Delta\Theta_4 = 0.306^\circ$. The ΔE array was at a distance of 3.03 m from the target. The seven scintillation plates, each of $500 \times 125 \times 10$ mm³, were placed horizontally and viewed on both sides by photomultipliers. The 28 blocks of the

E matrix with dimensions $120 \times 120 \times 200 \text{ mm}^3$ were arranged in seven rows just behind the ΔE plates.

The most important data from the RS were the angles (Θ_4, Φ_4) and the time of flight t_4 of particle 4. The particle trajectories were determined from the MWPC coordinates. The angular range in the off line evaluation was divided in 0.306° steps and — to eliminate the edge effects caused by the finite dimensions of the target — it was restricted to $-53.0^\circ \geq \Theta_4 \geq -61.0^\circ$ and $-5.8^\circ \leq \Phi_4 \leq 5.8^\circ$. The time of flight was obtained from the time signals of the ΔE detectors, measured relative to the start given by SPES IV. The accuracy of the measurement was checked through the kinematic relation $t_4(\Theta_4)$, the uncertainty in determination of t_4 turned out to be nearly 1 ns. The kinetic energy T_4 of the protons was determined either from t_4 or it was calculated from Θ_4 using the kinematical relation. The low energy threshold of the proton detection was set by software to $T_{4\text{min}}=70 \text{ MeV}$ to minimize uncertainties caused by energy losses and multiple scattering. Besides the coordinate and time-of-flight information some other quantities were also determined from the RS data, mainly to identify the reaction products and to reduce background.

The experiment was performed at five different settings of the magnetic field in SPES IV, corresponding to different domains of p_3 with central values $p_{30}=1.6, 1.7, 1.8, 1.9,$ and $2.0 \text{ GeV}/c$, respectively. The momentum as well as the angular acceptances of the spectrometer were defined in the data evaluation process by software. At each setting the events were collected into five momentum bins of size $\Delta p_3/p_{30} = 0.01$ and into three angular bins with $\Delta\Theta_3 = 0.3^\circ$. In the vertical direction only one bin was defined with $\Delta\Phi_3 = 2.17^\circ$.

In the course of the data evaluation special tests were prescribed for each event. Only those events were accepted for which the chamber coordinates allowed unambiguous determination of the trajectory. Additional conditions were that the trajectory originated at the target and that its coordinates at the ΔE detector were close enough to those determined from the ΔE detector data and from the position of the firing E detectors. The requirement of correct $\Delta E - t_4$ correlation was also used to define reliably the reaction events. After the filtering procedure about 23% of the triggered events remained as true ones. The combined efficiency of the detectors and of the data processing was about 80% which was checked by Monte Carlo simulations. The background measured by means of an empty target cell was $\sim 2\text{--}3\%$. After these corrections the absolute value of the cross section was calculated with about 25% systematic error. The relative errors of the measured distributions were practically the statistical ones.

III. EXPERIMENTAL RESULTS

Because the absolute value of the reaction cross section has marked dependence on p_3 as well as on Θ_3 , it was determined separately in the 15 bins characterized by the five and the three domains of these variables, as given in Sec. II. On the other hand, a similar distinction in

the Φ_3 and Φ_4 variables was not necessary owing to the relative insensitivity of the cross section on them. In the different momentum and angular bins the shape of the measured distributions was found to be similar, therefore in this section only data belonging to the central values p_{30} and Θ_{30} will be presented. When the number of events in a bin was too low, the content of the adjacent bins was averaged in order to reduce the statistical error.

The two-dimensional distributions of the events in the $[\Theta_4, t_4]$ coordinate plane are shown in Fig. 1 measured at the five p_{30} momenta. The distributions are concentrated along curves defined by the kinematics of the reaction. At $p_{30} = 1.6$ and $1.7 \text{ GeV}/c$ only the events with high T_4 (low t_4) are within the energy and angular acceptances of the RS, at higher p_{30} 's the spectra are accepted up to the kinematic limits of the reaction.

The fivefold differential cross section was calculated as

$$\frac{d^5\sigma}{dp_3 d\Omega_3 d\Omega_4} = C_{\text{exp}} \frac{N_p(\Theta_4)}{\Delta p_3 \Delta\Theta_3 \Delta\Phi_3 \Delta\Phi_4 \Delta\Theta_4}, \quad (3)$$

with $C_{\text{exp}} = 1/n_B n_T \epsilon$. The factor n_B is the beam intensity, n_T is the number of target nuclei per unit area, and the factor ϵ contains the inefficiency of the detectors and of the data filtering process.

The quantity $N_p(\Theta_4)$ is the number of protons detected by RS at Θ_4 in the $\Delta\Theta_4$ bin. This number was obtained from the two-dimensional $N_p(\Theta_4, t_4)$ spectra by summing the events at Θ_4 along the t_4 direction and subtracting the background. In practice, this was done by fitting the data with a Gaussian superimposed on a linear function. This procedure was effective through the whole angular range for the $p_{30}=1.6$ and $1.7 \text{ GeV}/c$ spectra; at higher momenta the backbending of the spectra at the kinematical limits allowed unambiguous determination of the cross section only below an arbitrarily chosen maximum angle. The experimental cross sections related to this high T_4 arm of the spectra are given in Table I.

To evaluate the experimental data in the lower T_4 region, near the kinematical limit, instead of the conventional quantity given in (3) the differential cross section

$$\frac{d^5\sigma}{dp_3 d\Omega_3 d\Phi_4 dT_4} = C_{\text{exp}} \frac{N_p(t_4)}{\Delta p_3 \Delta\Theta_3 \Delta\Phi_3 \Delta\Phi_4 \Delta t_4} \frac{dt_4}{dT_4} \quad (4)$$

was calculated being more appropriate to this situation. In this expression $N_p(t_4)$ is the number of recoil protons detected in the Δt_4 bin at t_4 and

$$\frac{dt_4}{dT_4} = \frac{t_4}{m_4 \gamma_4 (\gamma_4^2 - 1)} \quad (5)$$

with $\gamma_4 = E_4/m_4$. In the evaluation process $\Delta t_4 = 1 \text{ ns}$ was used and $N_p(t_4)$ was obtained by summation of the spectrum along Θ_4 . These cross sections are presented in Table II as a function of T_4 .

According to the general theory of reactions with multiparticle final states both cross sections (3) and (4) are in direct relation with the transition matrix element $|A|^2$ of the reaction through the kinematic factors K_Θ and K_T :

$$\begin{aligned}
 |A|^2 &= \frac{1}{K_\Theta} \frac{d^5\sigma}{dp_3 d\Theta_3 d\Phi_3 d\Phi_4 d\Theta_4} \\
 &= \frac{1}{K_T} \frac{d^5\sigma}{dp_3 d\Theta_3 d\Phi_3 d\Phi_4 dT_4},
 \end{aligned}
 \quad (6)$$

where

$$K_\Theta = \frac{p_3^2 p_4^2}{32(2\pi)^5 m_2 p_1 E_3 (p_4 E_5 - E_4 p_5 \cos \Theta_{45})} \quad (7a)$$

and

$$K_T = \frac{p_3^2}{32(2\pi)^5 m_2 p_1 p E_3 \sin \Theta_{40}}. \quad (7b)$$

In these expressions $\mathbf{p} = \mathbf{p}_1 - \mathbf{p}_3$ and Θ_{40} and Θ_{45} are the angles between the directions of \mathbf{p}_4 and \mathbf{p} and \mathbf{p}_4 and \mathbf{p}_5 , respectively in the horizontal plane. [Note in order to match the experimental layout, these formulas are related — in an unconventional way — to a spherical coordinate system with its axis perpendicular to the

horizontal plane, and the notations Θ_i for azimuthal and $(90^\circ - \Phi)$ for polar angles were used respectively.]

The transition matrix elements calculated according to (6) are displayed in Fig. 2 as a function of T_4 . The lines represent theoretical matrix elements (see below).

IV. DISCUSSION AND CONCLUSIONS

The experimental results are discussed in this section on the basis of the model including IA and NN rescattering. The initial goal of the experiment, based on *a priori* assumed dominance of IA, was to deduce the D_{dnp} amplitude of the dnp vertex in dependence on the mass of the virtual nucleon $t_{15} = (p_5 - p_1)^2$ or, what is the same, on the internal momentum q of nucleon in dnp -vertex $t_{15} = m_d^2 + m^2 - 2m_d\sqrt{m^2 + q^2}$. The graph of Fig. 3 represents the pole term in the invariant amplitude A caused by one nucleon exchange

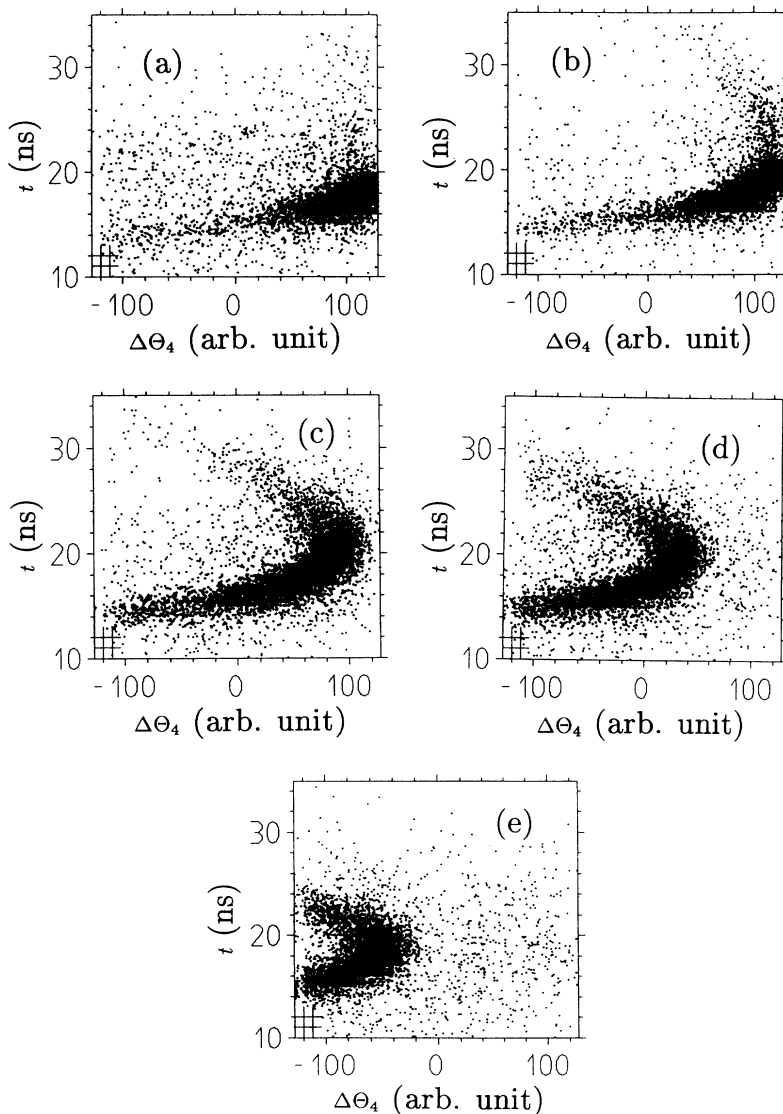


FIG. 1. Two dimensional spectra of the measured events in the $[t_4, \Theta_4]$ coordinate plane. (a) $p_3 = 1.6$ GeV/c, (b) $p_3 = 1.7$ GeV/c, (c) $p_3 = 1.8$ GeV/c, (d) $p_3 = 1.9$ GeV/c, (e) $p_3 = 2.0$ GeV/c.

TABLE I. Fivefold differential cross sections in the angular variable using Eq. (3), in mb/(sr² GeV) units.

Θ_4 (deg)	p_3 (GeV/c)				
	1.6	1.7	1.8	1.9	2.0
53.1	9.3 ± 1.7	7.4 ± 1.3	4.0 ± 0.5	4.2 ± 0.5	5.0 ± 0.3
53.4			5.0 ± 0.5	4.6 ± 0.5	5.5 ± 0.3
53.7	10.9 ± 1.8	7.4 ± 1.3	6.6 ± 0.6	5.3 ± 0.6	6.8 ± 0.4
54.0			7.3 ± 0.7	5.7 ± 0.6	7.9 ± 0.4
54.3	10.3 ± 1.8	9.1 ± 1.5	7.9 ± 0.7	6.7 ± 0.6	8.4 ± 0.4
54.6			7.7 ± 0.7	7.0 ± 0.7	10.4 ± 0.5
54.9	13.3 ± 2.0	9.5 ± 1.5	8.9 ± 0.7	9.3 ± 0.8	
55.2			9.8 ± 0.8	9.4 ± 0.8	
55.5	11.5 ± 1.9	16.8 ± 2.0	12.8 ± 0.9	12.8 ± 0.9	
55.8			14.1 ± 0.9	13.3 ± 0.9	
56.1	20.1 ± 2.5	24.0 ± 2.4	15.9 ± 1.0	15.7 ± 1.0	
56.4			20.7 ± 1.1	17.4 ± 1.0	
56.7	15.7 ± 2.2	25.1 ± 2.4	21.3 ± 1.1	20.7 ± 1.1	
57.0			28.4 ± 1.3	23.8 ± 1.2	
57.3	25.2 ± 2.8	38.6 ± 3.0	34.5 ± 1.4	28.4 ± 1.3	
57.6			39.3 ± 1.5	31.9 ± 1.4	
57.9	45.7 ± 3.8	50.7 ± 3.5	52.9 ± 1.8		
58.3		76.6 ± 4.2	61.8 ± 1.9		
58.6	69.9 ± 4.7	97.5 ± 4.8	70.3 ± 2.0		
58.9	66.9 ± 4.6	127.0 ± 5.5	86.0 ± 2.3		
59.2	116.0 ± 6.0	174.0 ± 6.4	98.3 ± 2.4		
59.5	184.0 ± 7.6	243.0 ± 7.6	118.0 ± 2.6		
59.8	267.0 ± 9.1	327.0 ± 8.8			
60.1	403.0 ± 11.2	431.0 ± 10.1			
60.4	605.0 ± 13.7	589.0 ± 11.8			
60.7	987.0 ± 17.5	750.0 ± 13.3			
61.0	1590.0 ± 22.2				
61.3	1810.0 ± 23.7				

$$A = \frac{M_{NN}(s_{34}, t_{24}, t_{15})D_{dnp}(t_{15})}{t_{15} - m^2} + B, \quad (8)$$

where the NN amplitude M_{NN} depends on the virtual mass t_{15} . The background B was approximated in our approach by taking into account nucleon rescatterings and the Δ excitation mechanism. More details can be found in Ref. [14]. Evidently, one could hope to extract D_{dnp} from $|A|^2$, neglecting the background B , which is more or less justified near the nucleon pole but is not justified away from it.

The t_{15} intervals covered in the experiment at different p_3 are determined by the $t_{24} = (p_4 - p_2)^2$ momentum transfer, which is directly related to the kinetic energy of the proton detected in RS, $t_{24} = -2mT_4$. The symbols in Fig. 2(a) show measured $|A|^2$ at five values of $p_3 = 1.6, 1.7, 1.8, 1.9,$ and 2.0 GeV/c as a function of T_4 , as well as the results of the calculation using the pole contribution (dashed lines) and including the background B (solid lines). The experimental points in Fig. 2 demonstrate in fact the evident deviation from the pole contribution at large T_4 for each p_3 , what is confirmed at least qualitatively by calculating the background processes. The experimental points at $T_4 \leq 0.2$ GeV for $p_3 = 1.8, 1.9,$ and 2.0 GeV/c do not confirm noticeable deviations from IA predicted by the model.

Figure 2(b) displays the variation of the mass t_{15} of

the virtual nucleon with T_4 . It is the closest to the pole value at $T_{40} \approx 0.15$ GeV for each p_3 moving off from the nucleon pole with increasing p_3 . The deviation from the pole increases above T_{40} and below as well even more rapidly. The insufficiency of the calculations to give satisfactory description of the experimental results in the whole investigated range of the kinematical variables,

TABLE II. Fivefold differential cross sections in the energy variables using Eq. (4), in mb/(sr^{3/2} GeV²) units.

T_4 (GeV)	p_3 (GeV/c)		
	1.8	1.9	2.0
0.333	5.1 ± 0.3	1.4 ± 0.1	
0.273	14.4 ± 0.5	4.9 ± 0.2	1.5 ± 0.1
0.230	30.6 ± 0.9	9.2 ± 0.3	2.9 ± 0.1
0.197	46.6 ± 1.2	10.8 ± 0.4	3.3 ± 0.1
0.171	54.7 ± 1.5	11.7 ± 0.4	3.7 ± 0.1
0.151	53.3 ± 1.6	11.3 ± 0.4	3.3 ± 0.1
0.134	46.1 ± 1.7	10.9 ± 0.5	3.2 ± 0.1
0.120	38.2 ± 1.6	9.9 ± 0.5	3.2 ± 0.2
0.109	31.0 ± 1.6	9.2 ± 0.5	
0.099	24.2 ± 1.5	6.7 ± 0.5	
0.091	16.7 ± 1.4	6.0 ± 0.5	
0.083	15.9 ± 1.4	5.2 ± 0.5	
0.077	9.1 ± 1.1		
0.072	8.1 ± 1.1		

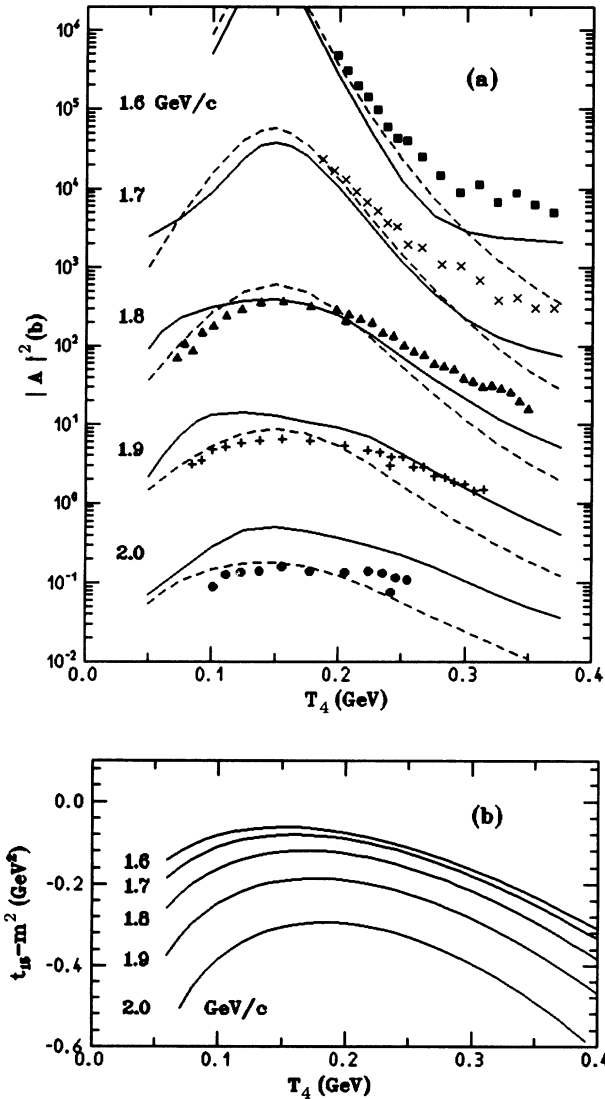


FIG. 2. (a) Experimental transition matrix elements of the $^1\text{H}(d, 2p)n$ breakup reaction (symbols) calculated according to Eq. (6) at $p_3 = 1.6, 1.7, 1.8, 1.9,$ and 2.0 GeV/c. The curves are theoretical calculations. Dashed line: pole contribution (IA), solid line: background corrected (IA+B). The data and curves for p_3 larger than 1.6 GeV/c were offset from one another by a factor of 10^{-1} for clarity. (b) Variation of the virtual nucleon mass with T_4 .

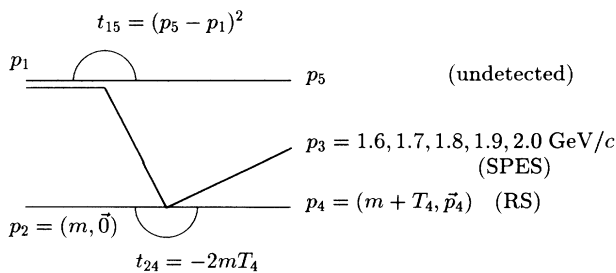


FIG. 3. Pole diagram of the impulse approximation.

may be connected to the rather strong dependence of the mass of the virtual nucleon on T_4 or t_{24} . More theoretical efforts are needed to understand the role of the off-shell effects in the $d + N$ reaction.

In order to make easier the comparison between the present results and those of previous experiments, we have calculated the experimental single particle momentum density $\rho(q)$ of the deuteron, based on the simple IA picture:

$$\rho(q) \equiv |\Phi(q)|_{\text{exp}}^2 = \frac{|A|^2}{K_{2B}(d\sigma/d\Omega)_{\text{c.m.}}} \quad (9)$$

Here $(d\sigma/d\Omega)_{\text{c.m.}}$ and K_{2B} are the free nucleon-nucleon scattering cross section and the two-body kinematical factor, respectively. The results for the different p_3 momenta are presented in Fig. 4 as a function of the internal momentum q , defined as the momentum of the spectator neutron transformed into the frame of the primary deuteron. The solid line represents $|\Phi(q)|^2$ calculated from the Paris potential.

The momentum densities displayed in Fig. 4(a) were

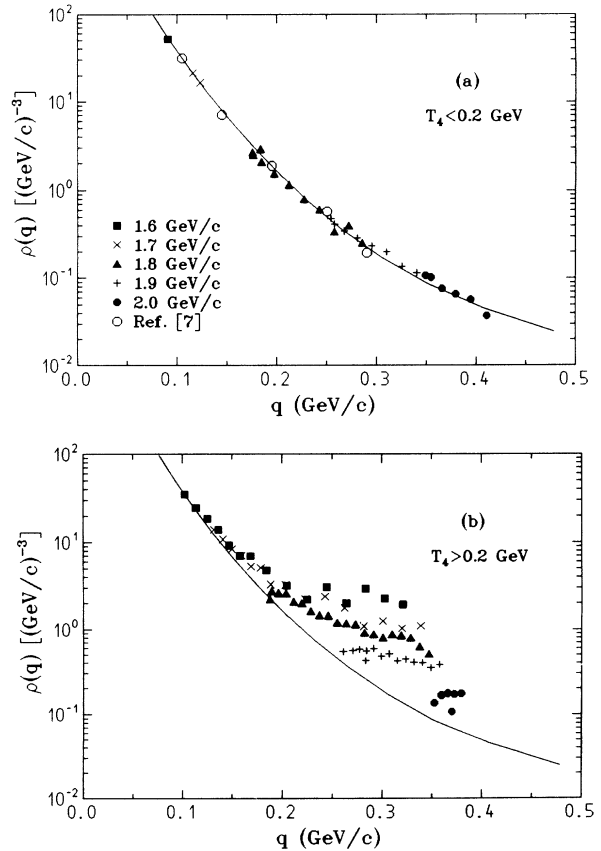


FIG. 4. Experimental single particle momentum density of the deuteron versus momentum q , measured at different momenta p_3 of the forward going protons. (a) Momentum densities related to low ($T_4 < 0.2$ GeV) and (b) to high ($T_4 > 0.2$ GeV) energies of the recoil protons. The solid line is the theoretical momentum density according to the Paris potential.

measured in the low energy region, at $T_4 < 0.2$ GeV. The experimental points are surprisingly close to the theoretical $|\Phi(q)|^2$ curve up to deuteron momenta as high as $q \approx 0.4$ GeV/c. This agreement with IA is in contradiction with the general situation because in previous experiments increased momentum densities were observed at q values above 0.2 GeV/c (Refs. [4–6] and [8–11]). Satisfactory agreement with theory was reported only in Ref. [7], where 1 GeV protons were used as bombarding particles, and the kinematical conditions were close to the present ones. The results of Ref. [7] are also shown in Fig. 4(a) (with open circles) for comparison. The agreement with the present results and with the theory is remarkable.

Momentum densities measured in the high energy region, i.e., at $T_4 > 0.2$ GeV, are displayed in Fig. 4(b). In contrast to the low T_4 case, large deviations from the theoretical values can be observed. The situation is similar to that found in earlier works, i.e., at low q values, up to approximately 0.2–0.3 GeV/c; the effective momentum density is close to the theoretical one, but at higher momenta $\rho(q)$ exceeds it significantly. This behavior is roughly justified by the above calculations taking into account the different background processes.

The fact that the behavior of $\rho(q)$ depends so markedly on T_4 , suggests an alternative approach for treating the experimental material instead of calculating the experimental momentum density $\rho(q)$. Assuming that $|\Phi|^2$ describes correctly the momentum density in every kinematical condition an “effective” N - N interaction $(d\sigma/d\Omega)_{\text{eff}}$ can be defined on the basis of (9) as

$$\left(\frac{d\sigma}{d\Omega}\right)_{\text{eff}} = \frac{|A|^2}{K_{2B}|\Phi|^2}, \quad (10)$$

and the observed deviations can be attributed to the variations of this effective N - N cross section on T_4 or t_{24} .

In Fig. 5 the related invariant cross section

$$\left(\frac{d\sigma}{dt}\right) = \frac{4\pi}{s - 4m_4^2} \left(\frac{d\sigma}{d\Omega}\right)_{\text{eff}} \quad (11)$$

is displayed as the function of the four-momentum transfer $t_{24} = -2mT_4$. The experimental points are effective cross sections obtained by using (10) and (11) while the solid lines were calculated from the known free pp cross sections.

The most striking feature in the figure is that the effective cross sections in the whole investigated kinematic region are distributed in a rather narrow band. At momentum transfers below ~ 0.35 (GeV/c) 2 , the effective cross section is very close to that of the free pp scattering whereas above it a sudden change can be observed and the cross sections take a more or less constant value. The introduction of the effective cross section for the analysis of the data is, of course, a phenomenological approach,

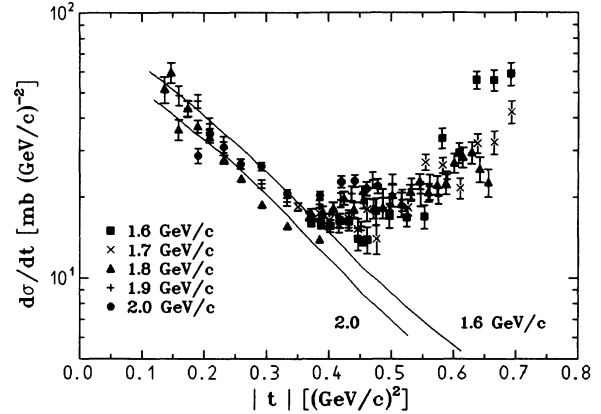


FIG. 5. Effective two-body cross sections $d\sigma/dt$ determined from the experimental data at different p_3 momenta. Solid lines are the free cross sections, belonging to $p_3 = 1.6$ and 2.0 GeV/c, respectively.

but it may turn the attention to an increased role of the four-momentum transfer in the breakup process in this kinematical region.

The breakup of the deuteron at intermediate energies seems to be a rather complex phenomenon. Besides rescattering, final state interaction, or excitation of resonances, the switching on of some new mechanisms at large momentum transfers should also be carefully examined. It would be important to explain, for example, why at low four-momentum transfers there does not appear the characteristic structure of the $\rho(q)$ distribution near $q \approx 0.2$ – 0.3 GeV/c observed in the high t region. This may be related to the fact that collisions with higher t tend to be more violent therefore they are influenced to varying extents by the internal nature of the interacting systems, e.g., by some substructures in the deuteron wave function like $|6q\rangle$ component proposed by Kobushkin and Vizireva [15].

To understand better the interplay of the different mechanisms in the pd interaction at high momentum transfers, detailed theoretical calculations are needed. The rather wide range of the kinematical conditions investigated in the present experiment provides a good basis for reliable theoretical analysis.

ACKNOWLEDGMENTS

We are grateful to the Saturne staff for their efficient and dedicated work in providing the excellent beam for this experiment. Partial funding for four of us (J. E., Z. F., P. K., and Z. S.) was provided by the Hungarian Science Foundation under OTKA Grant No. 1817.

- [1] M. Bernheim, A. Bussiere, J. Mougey, D. Royer, D. Tarnowski, S. Turck-Chieze, S. Frullani, G. P. Capitani, E. De Sanctis, and E. Jans, Nucl. Phys. **A365**, 349 (1981).
 [2] W. Mehnert, Ph.D. thesis, University of Bonn, 1984.

- [3] S. Turck-Chieze, P. Barreau, M. Bernheim, P. Bradu, Z. E. Meziani, J. Morgenstern, A. Bussiere, S. Frullani, F. Garibaldi, and J. Mougey, Phys. Lett. **142B**, 145 (1984).
 [4] C. F. Perdrisat, L. W. Swenson, P. C. Gugelot, E. T. Boschitz, W. K. Roberts, J. S. Vincent, and J. R. Priest,

- Phys. Rev. **187**, 1201 (1969).
- [5] T. R. Witten, M. Furič, G. S. Mutchler, C. R. Fletcher, N. D. Gabitzsch, G. C. Phillips, J. Hudomalj, L. Y. Lee, B. W. Mayes, J. Allred, and C. Goodman, Nucl. Phys. **A254**, 269 (1975).
- [6] V. Punjabi, K. A. Aniol, A. Bracco, C. A. Davis, M. B. Epstein, H. P. Gubler, W. P. Lee, D. J. Margaziotis, C. F. Perdrisat, P. F. Poffenberger, H. Postma, H. J. Sebel, A. W. Stetz, and W. T. H. van Oers, Phys. Rev. C **38**, 2728 (1988).
- [7] N. P. Aleshin, S. L. Belostotsky, Yu. V. Dotsenko, O. G. Grebenyuk, L. M. Kochenda, L. G. Kudin, N. P. Kuropatkin, S. I. Manayenkov, O. V. Miklukho, V. N. Nikulin, O. E. Prokofjev, A. Yu. Tsaregorodtsev, S. S. Volkov, J. Erő, J. Kecskeméti, Zs. Kovács, and Z. Seres, University of Leningrad Report No. 1259, 1987 (unpublished).
- [8] V. G. Ableev, D. A. Abdushukurov, S. A. Avramenko, Ch. Dimitrov, A. Filipkowski, A. P. Kobushkin, D. K. Nikitin, A. A. Nomofilov, N. M. Piskunov, V. I. Sharov, I. M. Sitnik, E. A. Strokovsky, L. N. Strunov, L. Vizireva, G. G. Vorobiev, and S. A. Zaporozhets, Nucl. Phys. **A393**, 491 (1983).
- [9] L. Anderson, W. Bruckner, E. Moeller, S. Nagamiya, S. Nissen-Meyer, L. Schroeder, G. Shapiro, and H. Steiner, Phys. Rev. C **28**, 1224 (1983).
- [10] C. F. Perdrisat, V. Punjabi, C. Lyndon, J. Yonnet, R. Beurtey, M. Boivin, A. Boudard, J. P. Didelez, R. Frascaria, T. Reposeur, R. Siebert, E. Warde, F. Plouin, P. C. Gugelot, and J. Y. Grossiord, Phys. Rev. Lett. **59**, 2840 (1987).
- [11] V. Punjabi, C. F. Perdrisat, P. Ulmer, C. Lyndon, J. Yonnet, R. Beurtey, M. Boivin, F. Plouin, J. P. Didelez, R. Frascaria, T. Reposeur, R. Siebert, E. Warde, A. Boudard, and P. C. Gugelot, Phys. Rev. C **39**, 608 (1989).
- [12] M. Garçon, in *Proceedings of the 7th International Conference on Polarization Phenomena in Nuclear Physics, Paris, 1990* [Colloq. Phys. **C6**, 61 (1990)].
- [13] E. Grorud, J. L. Laclare, A. Ropert, A. Tkatchenko, J. Banaigs, and M. Boivin, Nucl. Instrum. Methods **188**, 549 (1981).
- [14] J. Erő, Z. Fodor, P. Koncz, Z. Seres, C. F. Perdrisat, V. Punjabi, A. Boudard, B. Bonin, M. Garçon, R. Lombard, B. Mayer, Y. Terrien, E. Tomasi, M. Boivin, J. Yonnet, S. L. Belostotsky, O. G. Grebenuk, V. N. Nikulin, L. G. Kudin, H. C. Bang, and M. Youn, Report No. KFKI-1993-23/A, 1993 (unpublished); Proceedings of the International Symposium "DUBNA DEUTERON-93", Dubna, 1993, in Dubna Report No. E2-94-95, 1994 (unpublished).
- [15] A. B. Kobushkin and L. Vizireva, J. Phys. G **8**, 893 (1982).